Ukrainian Journal of Physical Optics
ISSUE 1
2026

Optical Vortex Generation Using a Glass Plate Bent by a Load Distributed Over a Finite Distance

O. Krupych, D. Adamenko, T. Dudok, I. Skab and R. Vlokh*

O.G.Vlokh Institute of Physical Optics, Ivan Franko National University of Lviv, 23 Dragomanov Str., Lviv, 79005, Ukraine
*Corresponding author: vlokh@ifo.lviv.ua

Received: 05.11.2025

Abstract. It has been experimentally demonstrated that an optical vortex produced using the bending of the glass plate with the aid of a load distributed over a finite distance of the upper surface of an optical glass plate is nearly canonical. It has been found that the generated dislocation of the phase front deviates from a pure screw dislocation toward a mixed screw-edge dislocation by no more than ~10%.

Keywords: optical vortex, flint glass, bending stress
UDC: 535.55
DOI: 10.3116/16091833/Ukr.J.Phys.Opt.2026.01102

1. Introduction

Optical vortices (OVs) are intriguing objects that have attracted the attention of scientists over the last few decades. Their quantum properties of possessing orbital angular momentum (OAM) l=0, ±1, ±2…make OVs the subject of deep study and application in a number of novel optical technologies. The vortex beam can be applied to quantum teleportation [1], quantum computing [2], optical beam focusing beyond the diffraction limit [3], communication systems, etc. Although OV generation methods are well developed, this issue still matters because different applications require different approaches.

Chronologically, the first method used for OV generation was the spiral phase plates method [4].Then the method of computer-synthesized holograms, which, in fact, represents a diffraction grating with a defect, which is manifested in the splitting of diffraction strips, has been developed [5].This method enables the generation of scalar-field OVs regardless of light polarization. Then, the method for creating polarization singularities in anisotropic media has been established. It has been found that so-called C-points (points in the polarization distribution where light polarization remains circular) give rise to OVs in the emerging beam. Such media include single-axial and biaxial crystals that generate OVs when a divergent circularly polarized optical beam propagates along their optical axes [6-8]. The appearance of OV in the outgoing beam, in this case, is caused by the axially symmetric distribution of anisotropy parameters within the angular aperture of the incident beam. Meanwhile, the anisotropic crystalline media remain homogeneous. The next step in the development of methods for OVs generation was the establishment of q-plates, liquid-crystalline plates with a defect in the director orientation at their center [9]. The q-plates enable the generation of OVs in a collimated optical beam with full spin-to-orbit (SAM-to-OAM) conversion efficiency by adjusting their thickness to the required phase difference. Further, many advanced technologies have been developed, including those based on spatial light modulators [10], metasurfaces [11,12], and techniques for generating vector and vortex-vector beams [13].

However, if to remind methods, based on the use of anisotropic media, except for those mentioned above, some techniques permit regulation of the efficiency of SAM-to-OAM conversion via externally applied fields [14-18]. These methods are based on the parametric optical effects, i.e., Pockels, Kerr, and piezo-optic effects. The general principles of OV generation in these cases are the same as in the q-plates, i.e., creation of the topological defect of optical indicatrix orientation in crystalline media subjected to the inhomogeneous electric field or mechanical stress. However, in the last cases, one can operate the efficiency of SAM-to-OAM conversion by the magnitude of the applied field [19,20]. Among such methods is crystal beam bending [18]. The advantage of this method is that, as the working element, one can use not only crystals but also amorphous materials. Recently, we experimentally demonstrated that when a concentrated and fully distributed load is applied to the entire upper surface of the sample, OVs can be generated [18]. But such conditions lead to the appearance of strongly anisotropic OVs. Moreover, the concentrated load leads to the appearance of two topological defects of optical indicatrix orientation with opposite signs [18]. The preferred approach in this case is to use a load distributed over a finite distance on the upper surface of the sample, which should yield a canonical single-charged OV. Therefore, the aim of the present work is the experimental verification of this suggestion.

2. Experimental methods

To induce bending stress distributed over a specific distance on the upper surface of the glass rod, we used the sample-loading scheme shown in Fig. 1.

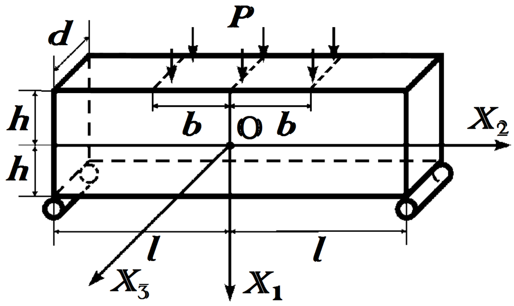

Fig. 1. Scheme of application of load distributed over the distance *2b* on the upper sample surface.

In our experiment, we have used flint glass (Φ1, which is close to F2 glass in SCHOTT classification) with the refractive index equal to n=1.6169 and stress-optic coefficient $B = n^3(\pi_{11} - \pi_{12})/2 = n^3\pi_{66}/2 = 2.95\times10^{-12}\ \mathrm{m^2/N}$ at λ = 550 nm [21]. The parameters of the glass plate and the experimental setup (Fig. 1) were $2h$ = 5 mm, d = 41 mm, $2b$ = 5mm, and $2l$ = 36 mm.

Let us consider the load distributed over the distance $2b$ on the upper sample surface (see Fig. 1). According to the theory of strength of materials [22,23] the induced components of the mechanical stress tensor and the moment of inertia can be written as:

$$\sigma_2 = \frac{M}{J}X_1,\ \sigma_6 = \frac{Q}{2J}\left(h^2 - X_1^2\right),\ J = \frac{2dh^3}{3}, \tag{1}$$

respectively. Here, J is the moment of inertia of the cross-section of a rectangular glass element relative to the neutral X_3 axis; Q and M are, respectively, the transverse force and bending moment. In the range $-l < X_2 < -b$, we have that

$$Q = \frac{P}{2},\ M = \frac{P}{2}\left(l + X_2\right), \tag{2}$$

where P is the load along the X_1 axis. The stress tensor components for this case become

$$\sigma_2 = \frac{3P}{4dh^3} X_1\left(l + X_2\right),\ \sigma_6 = \frac{3P}{8dh^3}\left(h^2 + X_1^2\right). \tag{3}$$

Then the birefringence and the angle of optical indicatrix rotation are given by

$$\Delta n = \frac{3PB}{4dh^3}\sqrt{X_1^2\left(l + X_2\right)^2 + \left(h^2 + X_1^2\right)^2}, \tag{4}$$

$$\tan\left(2\zeta\right) = -\frac{h^2 - X_1^2}{X_1\left(l + X_2\right)}. \tag{5}$$

The relations relevant for the range $b < X_2 < l$ are as follows:

$$Q = -\frac{P}{2},\ M = \frac{P}{2}\left(l - X_2\right), \tag{6}$$

$$\sigma_2 = \frac{3P}{4dh^3} X_1\left(l + X_2\right),\ \sigma_6 = \frac{3P}{8dh^3}\left(h^2 + X_1^2\right), \tag{7}$$

$$\Delta n = \frac{3BP}{4dh^3}\sqrt{X_1^2\left(l - X_2\right)^2 + \left(h^2 - X_1^2\right)^2}, \tag{8}$$

$$\tan\left(2\zeta\right) = -\frac{h^2 - X_1^2}{X_1\left(l - X_2\right)}. \tag{9}$$

Notice that relations (4), (5), (8), (9) are similar to formulae, which describe the birefringence and the optical indicatrix rotation angle distributions under the concentrated load [18].

Apart from the ranges mentioned above, there exists another range $-b < X_2 < b$, for which one can get

$$Q = -\frac{P}{2b} X_2,\ M = \frac{P}{4b}\left(2lb - b^2 - X_2^2\right). \tag{10}$$

Then we will have

$$\sigma_2 = \frac{3P}{8bdh^3} X_1\left(2lb - b^2 - X_2^2\right),\ \sigma_6 = -\frac{3P}{8bdh^3} X_2\left(h^2 - X_1^2\right), \tag{11}$$

while the birefringence and the optical indicatrix rotation angle read as

$$\Delta n = \frac{3PB}{8bdh^3}\sqrt{X_1^2\left(2lb - b^2 - X_2^2\right)^2 + 4X_2^2\left(h^2 - X_1^2\right)^2}, \tag{12}$$

$$\tan\left(2\zeta\right) = \frac{2X_2\left(h^2 - X_1^2\right)}{X_1\left(2lb - b^2 - X_2^2\right)}. \tag{13}$$

Formulas (12) and (13) can be written in polar coordinates, which are related to rectangular coordinates X_1 and X_2 as $X_1 = \rho\cos\varphi$ and $X_2 = \rho\sin\varphi$ as:

$$\Delta n = \frac{3PB}{8bdh^3}\rho\sqrt{\begin{aligned}&\left(2lb - b^2 - \rho^2\sin^2\varphi\right)^2\cos^2\varphi \\ &+4\left(h^2 - \rho^2\cos^2\varphi\right)^2\sin^2\varphi\end{aligned}}, \tag{14}$$

$$\tan(2\zeta) = 2\frac{h^2 - \rho^2\cos^2\varphi}{2lb - b^2 - \rho^2\sin^2\varphi}\tan\varphi\ . \tag{15}$$

Under the condition

$$2\frac{h^2 - \rho^2\cos^2\varphi}{2lb - b^2 - \rho^2\sin^2\varphi} = 1, \tag{16}$$

fomula (15) yields in $\tan(2\zeta) = \tan\varphi$ or $\zeta = \varphi / 2$ – i.e. we deal with the pure screw dislocation of the phase front, which leads to the appearance of the canonical vortex having the unit charge. Under the same conditions, the spatial birefringence distribution is given by a conical surface, $\Delta n \sim \rho$. Notice that Eq. (16) can be satisfied only approximately. The exact satisfaction of Eq. (16) can be realized only when $\rho = 0$.

The OV has been generated using the sample subjected to bending stresses, which is placed between crossed circular polarizers. This standard technique has been described, e.g., in our works [16,14]. Here, we only note that the doughnut mode in this scheme must be filtered by a circular analyzer with polarization rotation handedness opposite that of the incident light. The optical retardation and the azimuthal orientation of the polarization ellipse of the outgoing beam have been studied using an imaging polarimeter described in detail in our work [24].The interference fringes were obtained using a Mach-Zehnder interferometer, in which the sample loaded by the bending stress was placed in the probe arm. At the same time, the reference beam contained an objective lens for the creation of the spherical wavefront. As the light source, a He-Ne laser (λ=632.8 nm) has been used.

3. Results and discussion

As seen (Fig. 2), the central part of the polarimetric image obtained with crossed circular polarizers at a load of 287.4 N appears dark. This dark region is surrounded by a bright field. A dark spot at the center usually indicates the presence of an optical wavefront singularity.

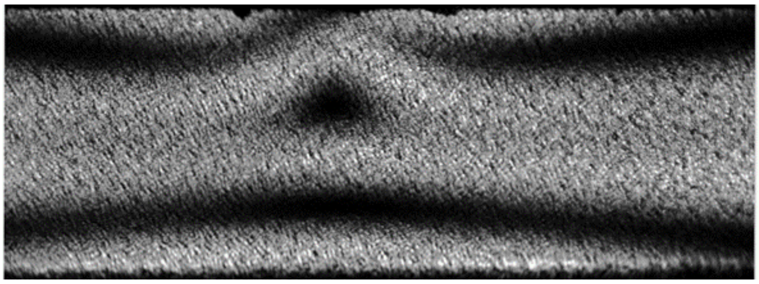

Fig. 2. The polarimetric image, obtained using crossed circular polarizers (P=287.4 N).

For its verification, we have carried out a polarimetric experiment in order to obtain the maps of azimuth and ellipticity of polarization of the emerged light from the loaded sample. As one can see (Fig. 3a,b), the map of azimuth at the load equal 0 N is homogeneous. However, the map of ellipticity shows deviation from 45 deg in the upper part of the sample. This can be caused by residual stress in the glass.

At the application of the load equal to 287.4 N, one can observe the appearance of polarization singularity in the central part of the map (Fig. 3c). The azimuth of the ellipse of light polarization rotates by 180 deg around the polarization singularity when the tracing angle φ is changed by 360 deg (Fig. 4). Such behavior corresponds to a topological defect in the optical indicatrix orientation, with a strength of ½.

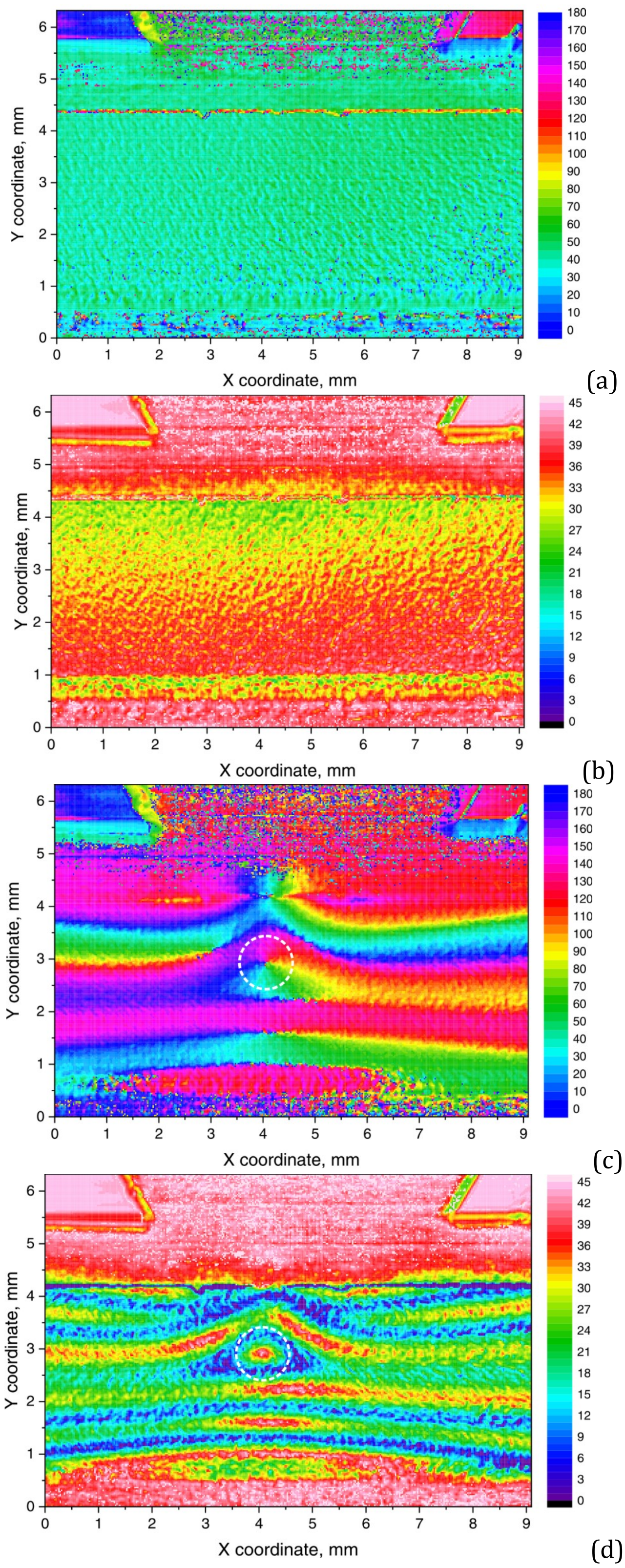

Fig. 3. The maps of azimuth (a, c) and ellipticity angle of outgoing beam at *P*=0 N (a, b) and *P*=287.4 N (c, d). The white circle is the tracing contour (see Fig.4)

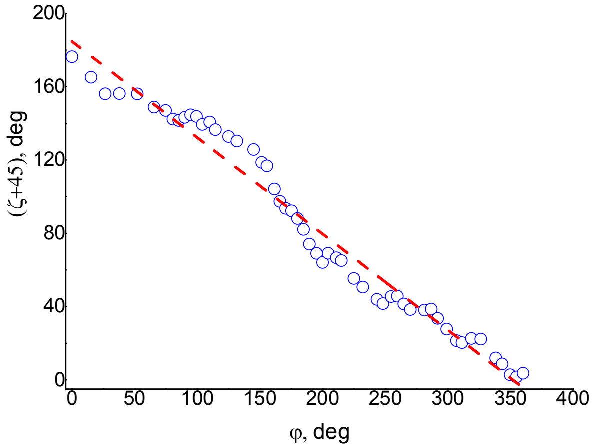

Fig. 4. Dependence of the azimuth of polarization ellipse orientation (the angle of optical indicatrix rotation is shifted by 45 deg with respect to the azimuth of polarization ellipse orientation) around the center of the topological defect on the tracing angle φ at a distance from the topological defect center of $\rho = 0.5$ mm .

The dependence of angle $\zeta + 45$ deg is almost linear, with the maximal deviation from linear fitting on about 10 deg. The linear fitting coefficient of determination is equal to R^2=0.972, and the standard deviation does not exceed 2.65 deg. It means that the generated dislocation of the phase front deviates from a pure screw dislocation toward a mixed screw-edge dislocation by no more than ~10%.

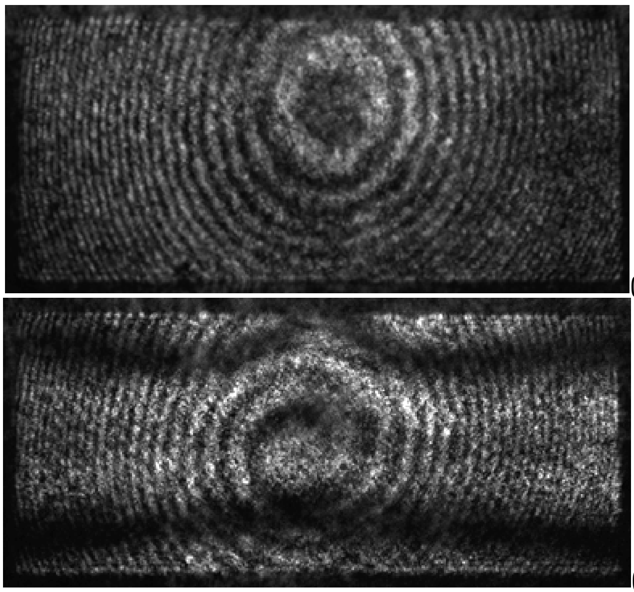
(a)
(b)

Fig. 5. The interferograms, obtained at the load equal to P=0 N (a) and P=230.9 N.

The ellipticity of the polarization of the outgoing light (Fig. 3d) at the coordinates of topological defect existence is exactly equal to 45 deg, corresponding to the circularly polarized light with the opposite sign with respect to the incident one. This topological defect is surrounded by an elliptical, but is close to the circular - green region with an ellipticity angle of ~20 deg. The blue region corresponding to the zero angle of ellipticity is deformed into a triangle. The existence of the bending-induced topological defect in the optical indicatrix orientation necessarily has to lead to almost canonical OV generation via spin-orbit conversion when the spin angular momentum of incident photons is $s=\pm1$. In fact, it is so. As seen, the interference fringes for the case of interference between the probe beam and the reference beam are circular for a load of 0 N and spiral for a load of 230.9 N (Fig. 5). Therefore, we have experimentally demonstrated that bending stress induced by a distributed load on the upper surface of the glass sample can lead to the generation of almost canonical OV.

4. Conclusion

In the present work, it has been experimentally shown that the generated OV, obtained by bending a glass plate and distributing the load over a finite distance on the upper surface, is almost canonical, with a small deviation toward a mixed screw edge dislocation of the phase front. On the other hand, the piezo-optic coefficient of flint glass is comparatively low, leading to relatively high loads that induce $\lambda/2$ retardation. From this point of view, the polycarbonate is a promising material due to its high value of $\pi_{66}= -39.2$ m^2/N [25,26].

Funding. This work was supported by the Ministry of Education and Science of Ukraine (project # 0124U000979).

Conflict of interest. Authors declare no conflict of interest.

References

1. Suciu, Ş., Bulzan, G. A., Isdrailă, T. A., Pălici, A. M., Ataman, S., Kusko, C., & Ionicioiu, R. (2023). Quantum communication networks with optical vortices. *Physical Review A*, *108*(5), 052612.
2. Hua, C., Halász, G. B., Dumitrescu, E., Brahlek, M., & Lawrie, B. (2021). Optical vortex manipulation for topological quantum computation. *Physical Review B*, *104*(10), 104501.
3. Edrei, E., & Scarcelli, G. (2020). Optical focusing beyond the diffraction limit via vortex-assisted transient microlenses. *ACS Photonics*, *7*(4), 914-918.
4. Beijersbergen, M. W., Coerwinkel, R. P. C., Kristensen, M., & Woerdman, J. P. (1994). Helical-wavefront laser beams produced with a spiral phaseplate. *Optics Communications*, *112*(5-6), 321-327.
5. Carpentier, A. V., Michinel, H., Salgueiro, J. R., & Olivieri, D. (2008). Making optical vortices with computer-generated holograms. *American Journal of Physics*, *76*(10), 916-921.
6. Volyar, A., Shvedov, V., Fadeyeva, T., Desyatnikov, A. S., Neshev, D. N., Krolikowski, W., & Kivshar, Y. S. (2006). Generation of single-charge optical vortices with an uniaxial crystal. *Optics Express*, *14*(9), 3724-3729.
7. Brasselet, E., Izdebskaya, Y., Shvedov, V., Desyatnikov, A. S., Krolikowski, W., & Kivshar, Y. S. (2009). Dynamics of optical spin-orbit coupling in uniaxial crystals. *Optics Letters*, *34*(7), 1021-1023.
8. Fadeyeva, T. A., Shvedov, V. G., Izdebskaya, Y. V., Volyar, A. V., Brasselet, E., Neshev, D. N., Desyatnikov, A.S., Krolikowski, W. & Kivshar, Y. S. (2010). Spatially engineered polarization states and optical vortices in uniaxial crystals. *Optics Express*, *18*(10), 10848-10863.
9. Marrucci, L., Manzo, C., & Paparo, D. (2006). Optical spin-to-orbital angular momentum conversion in inhomogeneous anisotropic media. *Physical Review Letters*, *96*(16), 163905.
10. Ostrovsky, A. S., Rickenstorff-Parrao, C., & Arrizón, V. (2013). Generation of the "perfect" optical vortex using a liquid-crystal spatial light modulator. *Optics Letters*, *38*(4), 534-536.
11. Ahmed, H., Kim, H., Zhang, Y., Intaravanne, Y., Jang, J., Rho, J., Chen, S. & Chen, X. (2022). Optical metasurfaces for generating and manipulating optical vortex beams. *Nanophotonics*, *11*(5), 941-956.
12. Du, J., & Wang, J. (2018). Dielectric metasurfaces enabling twisted light generation/detection/(de) multiplexing for data information transfer. *Optics Express*, *26*(10), 13183-13194.
13. Yan, X., Tao, X., Guo, M., Zhou, C., Chen, J., Shang, G., & Li, P. (2025, October). Vector Vortex Beams: Theory, Generation, and Detection of Laguerre–Gaussian and Bessel–Gaussian Types. In *Photonics* (Vol. 12, No. 10, p. 1029). MDPI.
14. Skab, I., Vasylkiv, Y., Smaga, I., & Vlokh, R. (2011). Spin-to-orbital momentum conversion via electro-optic Pockels effect in crystals. *Physical Review A – Atomic, Molecular, and Optical Physics*, *84*(4), 043815.
15. Vasylkiv, Y., Skab, I., & Vlokh, R. (2014). Generation of double-charged optical vortices on the basis of electro-optic Kerr effect. *Applied Optics*, *53*(10), B60-B73.
16. Skab, I., Vasylkiv, Y., Savaryn, V., & Vlokh, R. (2011). Optical anisotropy induced by torsion stresses in $LiNbO_3$ crystals: appearance of an optical vortex. *Journal of the Optical Society of America A*, *28*(4), 633-640.
17. Skab, I., Vasylkiv, Y., Zapeka, B., Savaryn, V., & Vlokh, R. (2011). Appearance of singularities of optical fields under torsion of crystals containing threefold symmetry axes. *Journal of the Optical Society of America A*, *28*(7), 1331-1340.

18. Skab, I., Vasylkiv, Y., & Vlokh, R. (2012). Induction of optical vortex in the crystals subjected to bending stresses. *Applied Optics*, *51*(24), 5797-5805.
19. Vasylkiv, Y., Skab, I., & Vlokh, R. (2013). Efficiency of electrooptic spin-to-orbital angular momentum conversion in crystals. *Optical Materials*, *35*(12), 2496-2501.
20. Vasylkiv, Y., Skab, I., & Vlokh, R. (2013). Efficiency of spin-to-orbit conversion in crystals subjected to torsion stresses. *Ukrainian Journal of Physical Optics*, (14,№ 1), 50-56.
21. Colourless optical glass. Physical and chemical properties. Basic parameters. State Standard 13659-78.
22. Timoshenko, S. P. (1958). *Strength of Materials: Part 1-Elementary*. Van Nostrand Reinhold Company.
23. Timoshenko, S. P. (1940). *Strength of Materials:* Part II: Advanced Theory and Problems. Van Nostrand Reinhold Company.
24. Krupych, O., Dudok, T., Skab, I., Nastishin, Y., Hrabchak, Z., Chernenko, A., Buluy, O., Zelenov, P., Nazarenko, V., Kurochkin, O. & Vlokh, R. (2025). Electric field controlled switching of an optical vortex charge with a liquid crystal cell. *Optics Communications*, *579*, 131593.
25. Waxler, R. M., Horowitz, D., & Feldman, A. (1979). Optical and physical parameters of Plexiglas 55 and Lexan. *Applied Optics*, *18*(1), 101-104.
26. Vasylkiv, Y., Smaga, I., Skab, I., & Vlokh, R. (2013). Efficient materials for spin-to-orbit angular momentum conversion using bending technique. *Ukrainian Journal of Physical Optics*, *14*(4), 200-209.

Krupych, O., Adamenko, D., Dudok, T., Skab, I., Vlokh, R. (2026). Optical Vortex Generation Using a Glass Plate Bent by a Load Distributed Over a Finite Distance**.** *Ukrainian Journal of Physical Optics*, *27*(1), 01102 – 01109. doi: 10.3116/16091833/Ukr.J.Phys.Opt.2026.01102

Анотація. *У цій роботі експериментально показано, що оптичний вихор, утворений за допомогою згинання скляної пластини при навантаженні, розподіленому вздовж скінченної відстані на верхній поверхні оптичної скляної пластини, є майже канонічним. Виявлено, що утворена дислокація фазового фронту відхиляється від чистої гвинтової дислокації у бік змішаної гвинтово-крайової дислокації не більше ніж на ~10%.*

Ключові слова: *оптичний вихор, оптичне скло Ф1, напруження згину*